Inorg. Chem. **2009**, *48*, 699−707

Preparation and Magnetic Properties of Iron(3+) Spin-Crossover Complexes Bearing a Thiophene Substituent: Toward Multifunctional Metallopolymers

Brandon Djukic,[†] Paul A. Dube,[‡] Fereidoon Razavi,[§] Takele Seda,[||] Hilary A. Jenkins,[‡] James F. Britten,[‡] and Martin T. Lemaire*[,†]

Department of Chemistry and Department of Physics, Brock University, St.Catharines, Ontario L2S 3A1, Canada, Department of Physics and Astronomy, Western Washington University, Bellingham, Washington 98225, and Brockhouse Institute for Materials Research, McMaster University, Hamilton, Ontario L8S 4M1, Canada

Received July 2, 2008

The synthesis of a new 3-ethynylthienyl-substituted QsalH ligand (QsalH is the short form for *N*-(8-quinolyl)salicylaldimine) (**ThEQsalH 3**), and the preparation, electronic, and magnetic properties of three homoleptic and cationic iron(3+) complexes containing this ligand with PF_6^- **4**, SCN^- **5**, and ClO_4^- **6** counteranions are reported. In all three complexes a spin-crossover is observed in the solid state by variable temperature magnetic susceptibility measurements and Mössbauer spectroscopy, indicating that the synthetic modification of the QsalH ligand has not significantly altered the electronics at the metal center. This includes the observation of a very rare $S = 5/2$ to 3/2 spin-crossover in a non-porphyrin iron(3+) complex **5**. The molecular structure and magnetic properties of an unusual iron(2+) complex **7** generated by reduction of complex **6** serendipitously during a recrystallization attempt in aerobic acetone solution is also reported. Complexes **4**−**6** feature iron(3+) reduction and oxidation of the thiophene ring at potentials of approximately −0.7 and +1.2 V (vs Fc), respectively.

Introduction

Considerable research efforts are currently focused on the preparation of molecule-based materials that feature two or more generally disparate properties, so-called "multifunctional materials". These include magnetic materials that also exhibit electrically conducting,[1−5] optical/luminescent,[6,7] porosity,[8,9] or ferroelectric[10,11] properties, just to name a few. Motivation for these studies stems, of course, from their multiproperty nature because this feature makes possible the production of systems in which one property may be controlled by another, that is, electrical transport properties may be controlled by other switching magnetic properties featured by the same material. These efforts are underway by a number of researchers attempting to utilize the spin-crossover[12−15] phenomenon in coordination complexes to

* To whom correspondence should be addressed. E-mail: mlemaire@brocku.ca.
[†] Department of Chemistry, Brock University.
[‡] McMaster University.
[§] Department of Physics, Brock University.
[||] Western Washington University.

(1) Coronado, E.; Galán-Mascarós, J. R.; Gómez-Garcia, C. J.; Laukhin, V. *Nature* **2000**, *408*, 447–449.
(2) Coronado, E.; Day, P. *Chem. Rev.* **2004**, *104*, 5419–5448.
(3) Hayashi, T.; Xiao, X.; Fujiwara, H.; Sugimoto, T.; Nakazumi, H.; Noguchi, S.; Katori, H. A. *Inorg. Chem.* **2007**, *46*, 8478–8480.
(4) Kosaka, Y.; Yamamoto, H. M.; Nakao, A.; Tamura, M.; Kato, R. *J. Am. Chem. Soc.* **2007**, *129*, 3054–3055.
(5) Dooley, B. M.; Bowles, S. E.; Storr, T.; Frank, N. L. *Org. Lett.* **2007**, *9*, 4781–4783.
(6) Paulsen, C.; Amabilino, D. B.; Veciana, J. *Angew. Chem., Int. Ed.* **2002**, *41*, 586.
(7) Chelebaeva, E.; Larionova, J.; Guari, Y.; Sa Ferreira, R. A.; Carlos, L. D.; Almeida Paz, F. A.; Trifonov, A.; Guérin, C. *Inorg. Chem.* **2008**, *47*, 775–777.
(8) Maspoch, D.; Ruiz-Molina, D.; Veciana, J. *Chem. Soc. Rev.* **2007**, *36*, 770–818.
(9) Milon, J.; Daniel, M.-C.; Kaiba, A.; Guionneau, P.; Brandès, S.; Sutter, J.-P. *J. Am. Chem. Soc.* **2007**, *129*, 13872–13878.
(10) Cui, H.; Wang, Z.; Takahashi, K.; Okano, Y.; Kobayashi, H.; Kobayashi, A. *J. Am. Chem. Soc.* **2006**, *128*, 15074–15075.
(11) Gu, Z.-G.; Zhou, X.-H.; Jin, Y.-B.; Xiong, R.-G.; Zuo, J.-L.; You, X.-Z. *Inorg. Chem.* **2007**, *46*, 5462–5464.
(12) Gutlich, P.; Garcia, Y.; Goodwin, H. A. *Chem. Soc. Rev.* **2000**, *29*, 419–427.
(13) Real, J. A.; Gaspar, A. B.; Muñoz, M. C. *Dalton Trans.* **2005**, 2062–2079.
(14) Nihei, M.; Shiga, T.; Maeda, Y.; Oshio, H. *Coord. Chem. Rev.* **2007**, *251*, 2606–2621.
(15) Sato, O.; Tao, J.; Zhang, Y.-Z. *Angew. Chem., Int. Ed.* **2007**, *46*, 2152–2187.

10.1021/ic801233x CCC: $40.75
Published on Web 11/21/2008

control electrical conductivity in electrocrystallized materials featuring both of these properties (spin-crossover and conductivity).[16−21] Recently Takahashi et al. have reported the structural, magnetic, and electrical transport properties of a variety of electrocrystallized salts containing iron(3+) complex cations that exhibit spin-crossover and conducting anions in the same lattice.[22,23] The goal is to obtain some degree of control over the magnitude of the conductivity exhibited by the anion via a through space "chemical pressure effect" induced by the structural changes that accompany the change in the spin state of the cation.

Our approach toward spin-crossover conductors featuring synergistic magnetic switching and electrical properties is to investigate the interplay between these properties, *in an intramolecular fashion*, within conducting thiophene polymers containing covalently attached spin-crossover complexes. Our synthetic plan includes the covalent attachment of a known spin-crossover complex to a thiophene heterocycle with an ethynyl spacer synthetically incorporated between these two units to help prevent steric congestion. We plan to generate polymeric materials by electropolymerization of these molecular precursors. With respect to the choice of the spin-crossover component of these materials, a number of homoleptic iron(3+) complexes containing the QsalH ligand (QsalH = *N*-(8-quinolyl)salicylaldimine) are known to exhibit spin-crossover,[24−26] and notable examples containing SCN^- or $SeCN^-$ counteranions feature very abrupt spin-transitions with wide thermal hysteresis loops. These fascinating properties result from increased cooperativity arising from strong intermolecular interactions generated by close π-π contacts in the solid state structures. These observations are in stark contrast to the majority of iron(3+) spin-crossover complexes, including those presented herein, which typically exhibit gradual spin-equilibria without thermal hysteresis.

An additional advantageous feature is that the QsalH framework is amenable to structural modification for tethering to the conjugated backbone. Our initial work has been focused on the synthesis of model complexes containing a structurally modified QsalH ligand and iron(3+) to investigate the effect of thiophene ring substitution on the electronic or magnetic properties of the $[Fe(Qsal)_2]^+$ moiety. Herein we report the synthesis of a 3-ethynylthienyl-substituted QsalH ligand (ThEQsalH), and the full characterization, electronic, and magnetic properties of three cationic iron(3+) complexes containing ThEQsalH, including the structural and magnetic characterization of an unusual iron(2+) complex obtained serendipitously from the iron(3+) complex.

Experimental Section

General Procedure. All reagents were commercially available and used as received unless otherwise stated. Deaerated and anhydrous solvents were obtained from a Puresolve PS MD-4 solvent purification system, and all air and/or moisture sensitive reactions were carried out using standard Schlenk techniques, unless otherwise stated. $^1H/^{13}C$ NMR spectra were recorded on a Bruker Advance 300 MHz spectrometer with a 7.05 T Ultrashield magnet using deuterated solvents. FT-IR spectra were recorded on a ThermoMattson RS-1 spectrometer as KBr discs or thin films on NaCl plates. EI and FAB mass spectra were obtained using a Kratos Concept 1S High Resolution E/B mass spectrometer, and ESI mass spectra were obtained using a Bruker HCT Plus Proteineer LC-MS. Room temperature UV/vis spectra were recorded on a ThermoSpectronic/Unicam UV-4 spectrophotometer as solutions in appropriate solvents. Spectra at 77 K were obtained as frozen ethanol glasses in 5 mm NMR tubes immersed in a liquid N_2 dewar flask. Elemental analyses were carried out by Guelph Chemical Laboratories LTD, Guelph, ON, Canada.

Electrochemical Measurements. Cyclic voltammetry (CV) and differential pulse voltammetry (DPV) experiments were performed with a Bioanalytical Systems Inc. Epsilon electrochemical workstation. Compounds were dissolved in anhydrous solvent (CH_2Cl_2 or CH_3CN) and deareated by sparging with dinitrogen gas for 20 min. Solution concentrations were approximately 10^{-3} M in analyte containing 0.1 M supporting electrolyte (Et_4NPF_6). A typical three-electrode setup was used including a platinum working electrode, Ag wire pseudoreference electrode, and a platinum wire auxiliary electrode. Ferrocene was used in all cases as an internal standard and was oxidized at a potential of +0.59 V in our set up; all potentials quoted are versus the ferrocene oxidation potential. Pulse amplitude of 50 mV, pulse width of 50 ms, and pulse period of 100 ms were applied in all DPV experiments. Scan rates for CV and DPV experiments were 100 and 40 mV/s, respectively.

X-ray Structure Determination and Powder Diffraction. Crystals of suitable size were mounted on a glass fiber. Data were collected at room temperature (293 K) on a SMART APEX II diffractometer with Mo Kα radiation (λ = 0.71073 Å) located at the McMaster Analytical X-ray Diffraction Facility (MAX). Data were processed using APEX v2.2.0 and solved by direct methods (SHELXS-97). All atoms were refined anisotropically except for residual solvent (acetone and water); hydrogen atoms were treated as riding on their constituent atoms and updated after each cycle of refinement. Disorder in the thiophene portions of each coordinated ligand between S1(A) and C21(A), and between S2(A) and C51(A) was modeled at 77% and 57% respectively; see Table 1 for crystallographic data. Disordered solvent water and acetone were removed from the lattice using the program SQUEEZE.

X-ray powder diffraction data for **5** were obtained with a Bruker APEX II diffractometer using Mo Kα radiation at 295 K and a detector-to-sample distance of 17 cm. X-ray powder diffraction data for **6** were obtained with a Bruker SMART 1K diffractometer, at 295 K, using Cu Kα radiation, and a detector-to-sample distance

(16) Takahashi, K.; Kawakami, T.; Gu, Z.; Einaga, Y.; Fujishima, A.; Sato, O. *Chem. Commun.* **2003**, 2374–2375.
(17) Dorbes, S.; Valade, L.; Real, J. A.; Faulmann, C. *Chem. Commun.* **2005**, 69–71.
(18) Takashi, K.; Cui, H.; Kobayashi, H.; Einaga, Y.; Sato, O. *Chem. Lett.* **2005**, *34*, 1240–1241.
(19) Faulmann, C.; Dorbes, S.; Garreau de Bonneval, B.; Molnár, G.; Bousseksou, A.; Gomez-Garcia, C. J.; Coronado, E.; Valade, L. *Eur. J. Inorg. Chem.* **2005**, 3261–3270.
(20) Pereira, L. C. J.; Gulamhussen, A. M.; Dias, J. C.; Santos, I. C.; Almeida, M. *Inorg. Chim. Acta* **2007**, *360*, 3887–3895.
(21) Faulmann, C.; Jacob, K.; Dorbes, S.; Lampert, S.; Malfant, I.; Doublet, M.-L.; Real, J. A. *Inorg. Chem.* **2007**, *46*, 8548–8559.
(22) Takahashi, K.; Cui, H.-B.; Okano, Y.; Kobayashi, H.; Einaga, Y.; Sato, O. *Inorg. Chem.* **2006**, *45*, 5739–5741.
(23) Takahashi, K.; Cui, H.-B.; Okano, Y.; Kobayashi, H.; Mori, H.; Tajima, H.; Einaga, Y.; Sato, O. *J. Am. Chem. Soc.* **2008**, *130*, 6688–6689.
(24) Oshio, H.; Kitazaki, K.; Mishiro, J.; Kato, N.; Maeda, Y; Takashima, Y. *J. Chem. Soc., Dalton Trans.* **1987**, 1341–1347.
(25) Hayami, S.; Gu, Z.-z.; Yoshiki, H.; Fujishima, A.; Sato, O. *J. Am. Chem. Soc.* **2001**, *123*, 11644–11650.
(26) Dickinson, R. C.; Baker, W. A.; Collins, R. L. *J. Inorg. Nucl. Chem* **1977**, *39*, 1531–1533.

Table 1. Crystallographic Data for **7**

formula	$C_{47}H_{32}FeN_4O_5S_2$
fw	852.74
dimensions (mm)	0.32 × 0.23 × 0.06
a (Å)	14.504(6)
b (Å)	17.778(7)
c (Å)	16.911(8)
cryst syst	monoclinic
α (deg)	90
β (deg)	109.377(10)
γ (deg)	90
volume (Å^3)	4113(3)
space group	$P2_1/n$
Z	4
μ (mm^{-1})	0.519
T (K)	296(2)
independent reflections	7522, $R_{int} = 0.063$
R_1	0.0527
wR_2	0.1409

of 5 cm. In both experiments the powder was mounted in a glass slide, and a 5 min still scan was recorded with the sample at $\omega = 20°$. For comparison, the X-ray powder diffraction pattern of **7** was calculated using the program Mercury 1.4.2.

Variable Temperature Magnetic Susceptibility Measurements and EPR Spectroscopy. Variable temperature magnetic susceptibility measurements were recorded on a superconducting quantum interference device (SQUID) magnetometer (Quantum Design MPMS) with a 5.5 T magnet (temperature range 1.8 to 400 K) in an external field of 5000 Oe. Samples were carefully weighed into gelatin capsules, with empty gelatin capsules above and below to eliminate background contributions from the gelatin, which were loaded into plastic straws, and attached to the sample transport rod. Diamagnetic corrections were made using Pascal's constants. Electron Paramagnetic Resonance (EPR) spectra were recorded as powders in quartz tubes on a BrukerElexsys E580 pulsed and CW X-band (9 GHz) spectrometer, equipped with a liquid helium cryostat.

Mössbauer spectroscopy. Mössbauer spectra were recorded with a constant-acceleration spectrometer (Wissel GMBH, Germany) in a horizontal transmission mode using a 50 mCi ^{57}Co source. A Janis SHI-850-1 closed cycle helium refrigerator cryostat was used for variable temperature measurements. All spectra were fitted by Lorentzian line shapes using NORMOS (Wissel GMBH) least-squares fitting program. The velocity scale was normalized with respect to metallic iron at room temperature; hence, all isomer shifts were recorded relative to metallic iron.

Synthesis

5-(Ethynyltrimethylsilyl)salicylaldehyde. 5-Bromosalicylaldehyde (4.650 g, 0.0231 mol), PPh_3 (0.121 g, 2 mol%), $Pd(PPh_3)_2Cl_2$ (0.324 g, 2 mol%), and CuI (0.132 g, 3 mol %) were combined with 150 mL of deareated anhydrous diisopropylamine. Ethynyltrimethylsilane (2.497 g, 0.0254 mol) was added last, and the mixture was heated to reflux for 4 h. The reaction was concentrated under reduced pressure, combined with pentane (300 mL), and then filtered through a celite pad. The solvent was removed by rotary evaporation to afford 4.945 g (99.8%) of light yellow powder. Mp: 121−124 °C. ^{1}H NMR ($CDCl_3$): *δ* 11.11 (s br, 1H), 9.87 (s, 1H), 7.73 (d, 1H, $J = 2$ Hz), 7.64 (dd, 1H, $J = 9$, 2 Hz), 6.97 (d, 1H, $J = 9$ Hz), 0.27 (s, 9H) ppm. ^{13}C NMR ($CDCl_3$): *δ* 196.0, 161.5, 140.1, 137.3, 120.3, 117.9, 115.1, 103.2, 93.2, −0.1 ppm. MS (EI): *m/z* 218 (M^+, %), 203 [$(M - CH_3)^+$, 100%]. FT-IR (KBr): 3427 (m), 3206 (w), 2957 (w), 2878 (w), 2150(m), 1668 (s), 1475 (s), 1377 (w), 1285 (s), 1245 (m), 1149 (s), 843 (s), 757 (m), 693 (m), 584 (w) cm^{-1}. Calcd for (found %) $C_{12}H_{14}O_2Si$: C, 66.03 (66.39); H, 6.47% (6.78).

5-Ethynylsalicylaldehyde (1). 5-Ethynyltrimethylsilylsalicylaldehyde (4.945 g, 0.0226 mol) was dissolved in THF (20 mL). Potassium hydroxide (1.268 g, 0.0226 mol) was dissolved in MeOH (10 mL) and added to the THF solution. The reaction mixture was stirred at room temperature overnight, and then the solvent was concentrated under reduced pressure. The residue was dissolved in $CHCl_3$ and washed with 0.05 M HCl (400 mL) and distilled water (400 mL). The organic phase was dried over $MgSO_4$, filtered, and the solvent was removed by rotary evaporation to obtain 3.26 g (98%) of light yellow powder. Mp: 115−118 °C. ^{1}H NMR ($CDCl_3$): *δ* 11.15 (br s, 1H), 9.89 (s, 1H), 7.75 (d, 1H, $J = 2$ Hz), 7.66 (d, 1H, $J = 9$, 2 Hz), 7.00 (d, 1H, $J = 9$ Hz), 3.06 (s, 1H) ppm. ^{13}C NMR ($CDCl_3$): *δ* 196.0, 161.8, 140.2, 137.5, 120.4, 118.2, 114.0, 81.9, 76.8 ppm. MS (EI): *m/z* 146 (M^+, 100%). FT-IR (KBr): 3427 (w), 3273 (s), 3010 (w), 2886 (w), 1663 (s), 1580 (m), 1477 (s), 1377 (m), 1290 (s), 1201 (s), 1140 (m), 910 (w), 847 (m), 766 (m), 720 (w), 643 (m), 579 (w), 453 (w) cm^{-1}. Calcd for (found %) $C_9H_6O_2$: C, 73.95 (74.12); H, 4.14% (4.07).

5-(3′-Ethynylthienyl)salicylaldehyde (2). 1 (1.000 g, 6.84 mmol), 3-bromothiophene (1.116 g, 6.84 mmol), PPh_3 (0.090 g, 5 mol %), $Pd(PPh_3)_2Cl_2$ (0.240 g, 5 mol %), and CuI (0.065 g, 5 mol%) were added to anhydrous and deareated THF (50 mL) containing diisopropylamine (0.97 mL). The reaction was stirred under reflux for 20 h, cooled to room temperature, and then concentrated under reduced pressure. The residue was combined with pentane (300 mL), and then filtered through a celite pad, concentrated to dryness, and the residue was dissolved in acetone. The solution was filtered, and concentrated to dryness again. The residue was dissolved in $CHCl_3$ and washed with 0.05 M HCl (200 mL) and distilled water (200 mL). The organic phase was dried over $MgSO_4$, filtered, and the solvent was removed by rotary evaporation to afford 0.843 g (54%) of light yellow powder. Mp: 95−95 °C. ^{1}H NMR ($CDCl_3$): *δ* 11.13 (br s, 1H), 9.91 (s, 1H), 7.77 (d, 1H, $J = 2$ Hz), 7.69 (dd, 1H, $J = 9$, 2 Hz), 7.54 (d, 1H, $J = 3$ Hz), 7.35 (dd, 1H, $J = 5$, 3 Hz), 7.22 (d, 1H, $J = 5$ Hz), 7.02 (d, 1H, $J = 9$ Hz) ppm. ^{13}C NMR ($CDCl_3$): *δ* 196.1, 161.4, 139.7, 138.8, 129.8, 128.7, 125.6, 121.9, 120.5, 118.2, 115.2, 87.0, 84.1 ppm. MS (EI): *m/z* 228 (M^+, 100%). FT-IR (KBr): 3427 (w), 3095 (w), 2921 (w), 2854 (w), 1656 (s), 1578 (w), 1480 (m), 1375 (w), 1286 (m), 1199 (w), 1115 (w), 957 (m), 867 (w), 801 (w), 742 (w), 686 (w), 624 (w), 575 (w), 521 (w), 446 (w) cm^{-1}. Calcd for (found %) $C_{13}H_8SO_2$: C, 68.41 (68.66); H, 3.54% (3.30).

ThEQsalH (3). 2 (0.293 g, 1.29 mmol) was dissolved in $CHCl_3$ (0.4 mL) and added to a solution of 8-aminoquinoline (0.185 g, 1.29 mmol) in ethanol (50 mL). The solution was stirred at room temperature for 72 h and then filtered. The solvent was removed by rotary evaporation to afford 0.431 g (93%) of crimson oil. ^{1}H NMR ($CDCl_3$): *δ* 14.45 (br s, 1H), 8.97 (dd, 1H, $J = 4$, 2 Hz), 8.93 (s, 1H), 8.19 (dd, 1H,

J = 8, 2 Hz), 7.75 (dd, 1H, J = 8, 2 Hz), 7.64−7.45 (m, 6H), 7.31 (dd, 1H, J = 8, 2 Hz), 7.20 (d, 1H, J = 5 Hz), 7.06 (d, 1H, J = 9 Hz) ppm. HRMS (EI +) calculated for $[C_{22}H_{14}ON_2S]^+$: 354.08361 found 354.08269. FT-IR (KBr): 3427 (m), 3038 (w), 1619 (s), 1495 (s), 1384 (m), 1284 (m), 1244 (w), 1161 (w), 1084 (w), 1054 (w), 891 (w), 827 (m), 787 (m), 754 (w), 595 (w), 469 (w) cm^{-1}. UV−vis ($CHCl_3$): λ_{max} (ε (M^{-1} cm^{-1})) 500 nm (285). Calcd for (found %) $C_{22}H_{14}ON_2S$: C, 74.56 (74.21); H, 3.99 (3.85); N, 7.91% (7.97).

Preparation of Complexes 4 and 5. 3 (0.489 g, 1.38 mmol) was suspended in MeOH (40 mL), combined with Et_3N (0.140 g, 1.38 mmol), and stirred for 10 min. $FeCl_3 \cdot 6H_2O$ (0.187 g, 0.690 mmol) was then added, and the solution was stirred for 1 h. An excess of $NaPF_6$ **4** (0.406 g, 2.42 mmol), or KSCN **5** (0.235 g, 2.42 mmol), were added, and the mixture was stirred overnight. Combining the mixtures with distilled water (250 mL) resulted in deep green microcrystalline precipitates that were filtered off, washed with water, pentane, and then dried.

$[Fe(3)_2]PF_6$ (4). Yield: 0.624 g (89.7%). MS (ESI +): m/z 762 [(M − PF_6)$^+$, 100%]. UV−vis (CH_3CN): λ_{max} (ε (M^{-1} cm^{-1})) 445 nm (insolubility of **4** precluded an accurate determination of ε). FT-IR (KBr): 3052 (w), 2920 (w), 1606 (s), 1574 (m), 1504 (m), 1455 (m), 1375 (m), 1307 (m), 1164 (w), 1089 (w), 842 (vs), 780 (w), 557 (w), 511 (w) cm^{-1}. Calcd for (found %) $C_{44}H_{26}O_2N_4S_2FePF_6$: C, 58.23 (58.53); H, 2.89 (3.00); N, 6.17% (5.84).

$[Fe(3)_2]$ SCN·2.5·H_2O (5). Yield: 0.497 g (87.2%). MS (ESI +): m/z 762 [(M − SCN)$^+$, 100%]. UV−vis (CH_3CN): λ_{max} (ε (M^{-1} cm^{-1})) 455 nm (insolubility of **5** precluded an accurate determination of ε). FT-IR (KBr): 3450 (m), 3052 (w), 2921 (w), 2053 (vs), 1607 (s), 1574 (s), 1503 (m), 1456 (s), 1376 (m), 1308 (m), 1164 (m), 1088 (w), 1038 (m), 927 (w), 828 (m), 782 (m), 677 (w), 547 (m), 511 (w) cm^{-1}. Calcd for (found %) $C_{45}H_{26}O_2N_5S_3Fe \cdot 2.5 \cdot H_2O$: C, 62.43 (62.91); H, 3.61 (3.18); N, 8.08% (7.45).

$[Fe(3)_2]ClO_4$ (6). 3 (0.397 g, 1.12 mmol) was dissolved in CH_2Cl_2 (10 mL), and a half-equivalent of $Fe(ClO_4)_3 \cdot 6H_2O$ (0.199 g, 0.56 mmol) dissolved in CH_3CN (15 mL) was added at room temperature in air. A dark precipitate formed immediately in the solution, to which an additional 25 mL of CH_3CN was added. The mixture was stirred for 2 h, and the dark maroon precipitate was isolated by vacuum filtration, washed with water, pentane, and dried. Yield: 0.343 g (71%). MS (ESI +): m/z 762 [(M − ClO_4)$^+$, 100%]. UV−vis ($CHCl_3$): λ_{max} (ε (M^{-1} cm^{-1})) 450 nm (4100). FT-IR (KBr): 3098 (w), 3063 (w), 1605 (s), 1573 (s), 1527 (m), 1503 (s), 1454 (m), 1397 (m), 1376 (m), 1306 (m), 1241 (w), 1190 (w), 1093 (vs), 829 (m), 782 (m), 760 w), 622 (m), 548 (w), 512 (w) cm^{-1}. Calcd for (found %) $C_{44}H_{26}O_6N_4S_2FeCl$: C, 61.29 (61.25); H, 3.04 (3.01); N, 6.50% (6.31)

$Fe(3)_2 \cdot C_3H_6O \cdot 1.5H_2O$ (7). 6 (40 mg, 0.046 mmol) was stirred in acetone (20 mL) for 0.5 h. The solution was filtered and divided into two equal portions, which were left to stand open to air at room temperature. Black plate crystals formed by slow evaporation. MS (ESI +): 762 (M^+, 100%). UV−vis ($CHCl_3$): λ_{max} (ε (M^{-1} cm^{-1})) 445 nm (4400). FT-IR (KBr): 3063 (w), 2961 (w), 2922 (w), 2851 (w), 1605 (s), 1573 (s), 1504 (s), 1454 (m), 1376 (m), 1314 (m), 1260 (m), 1203 (m), 1164 (m), 1129 (m), 1088 (m), 825 (s), 777 (s), 623 (w), 551 (w), 511 (w) cm^{-1}. Calcd for (found %) $C_{47}H_{32}O_{4.5}N_4S_2Fe$: C, 66.83 (64.76); H, 4.18 (3.99); N, 6.63% (6.04).

Scheme 1. Synthesis of **3**[a]

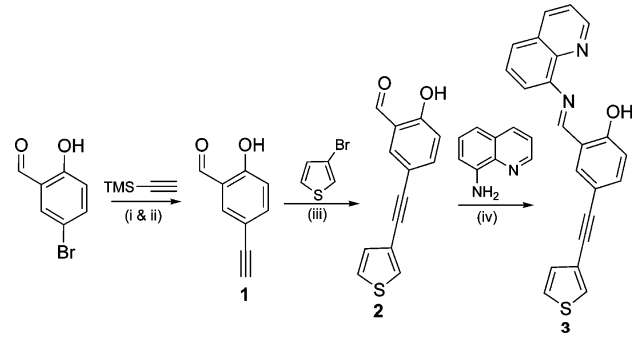

[a] Reagents and conditions, (i) 3 mol % CuI, 2 mol % $Pd(PPh_3)_2Cl_2$ and PPh_3 iPr_2NH, 4 hr reflux. (ii) KOH, MeOH/THF, 12 hr at RT. (iii) 5 mol % CuI, 5 mol % $Pd(PPh_3)_2Cl_2$ and PPh_3 iPr_2NH, THF 20 hr reflux. (iv) $CHCl_3$/EtOH, 72 hr at RT.

Results and Discussion

Ligand Synthesis, Coordination Chemistry, and Structural Studies. The ThEQsalH ligand **3** was prepared in four steps from the commercially available reagents 3-bromothiophene and 5-bromosalicylaldehyde (Scheme 1). Sonogashira cross-coupling between 5-bromosalicylaldehyde and ethynyltrimethylsilane afforded the protected acetylene precursor, which was deprotected by stirring overnight in base to afford acetylene **1**, following a procedure modified from that reported by Lin. [27] Another Sonogashira reaction between **1** and 3-bromothiophene afforded aldehyde precursor **2** as a yellow powder, which was condensed with 8-aminoquinoline to yield the modified QsalH ligand **3** as a crimson oil, which is somewhat hydrolytically unstable in solution but has been fully characterized. In the ^1H NMR spectrum of **3**, the hydroxyl proton is shifted downfield relative to the same proton in the aldehyde precursor (14.5 vs 11.3 ppm). The C=N stretch of the imine is observed at 1620 cm^{-1} in the FT-IR spectrum of **3**, and will undergo a small shift to lower energy upon metal coordination.

Homoleptic coordination complexes were generated by reaction of 2 equiv of **3** with hydrated iron(III) chloride in the presence of triethylamine, followed by metathesis with aqueous solutions containing an excess of $NaPF_6$ or KSCN to afford dark green precipitates of the PF_6 **4** or SCN **5** salts containing the $[Fe(\mathbf{3})_2]^+$ cation. Complex **6**, containing a perchlorate anion, was prepared by direct reaction of $Fe(ClO_4)_3 \cdot 6H_2O$ with 2 equiv of **3** in CH_2Cl_2/acetonitrile solution. All complexes are analytically pure and produce very clean ESI mass spectra, with the dominant $[Fe(\mathbf{3})_2]^+$ cation clearly observable and featuring the correct isotope distribution for the purported formulation (Supporting In-

(27) Chang, K.-H.; Huang, C.-C.; Liu, Y.-H.; Hu, Y.-H.; Chou, P.-T.; Lin, Y.-C. *Dalton Trans.* **2004**, 1731–1738.

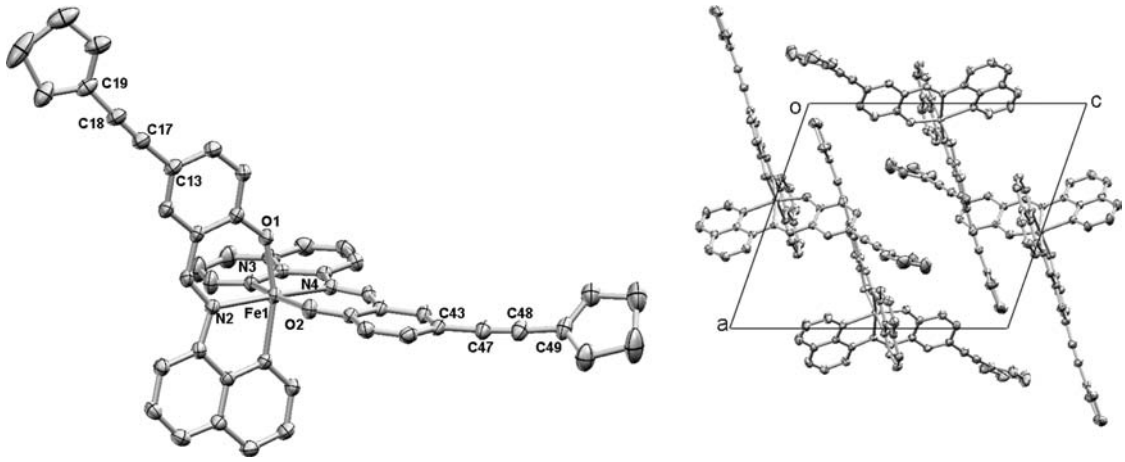

Figure 1. Left: Molecular structure of **7** (thermal ellipsoids at 30% probability). Right: Packing of **7** along *b* axis. Hydrogen atoms omitted for clarity.

formation, Figures S4−S6). The FT-IR spectra for each complex are very similar, with slight differences due to the absorptions of the different anionic component of the structures (Supporting Information, Figures S1−S3). Coordination is also indicated by a slight shift (∼15 cm^{-1}) in the C=N stretching frequency to lower energy in complexes **4**, **5**, and **6** relative to uncoordinated **3**. The visible spectra of complexes **4**−**6** in acetonitrile solution features an intense ligand-to-metal charge transfer (LMCT) absorption at approximately 450 nm, which is also observed for other reported $[Fe(Qsal)_2]^+$ complexes.[24−26] Unfortunately, repeated attempts to grow single crystals of complexes **4**, **5**, and **6** suitable for X-ray diffraction studies using a variety of different techniques and solvent combinations have been unsuccessful. On the basis of the structural data we have provided above, however, we are confident in the proposed formulations for complexes **4**−**6**. Curiously, recrystallization of **6** in aerobic acetone solution generated black plate crystals of the reduced iron(2+) complex **7** as an acetone and water solvate. An Oak Ridge Thermal Ellipsoid Plot (ORTEP) diagram of the molecular structure of **7** is shown (Figure 1, left).

In the structure of **7** the iron center features the expected pseudo-octahedral coordination geometry, with two anionic molecules of **3** coordinated at three meridional positions through its donor quinolyl and imine N atoms, and the phenolate O. Coordinate bond lengths clearly indicate the +2 oxidation state for the metal, with Fe−N lengths greater than 2.13 Å in all cases (Table 2), and each Fe−O bond greater than 1.9 Å. In other similar structurally characterized iron complexes with the parent Qsal anion, but featuring iron(3+), Fe−N coordinate bond lengths are all less than 2 Å and Fe−O bond lengths are less than 1.9 Å.[25] No perchlorate anion is present in the structure of **7**. The mechanism for the formation of this unusual species is unclear and currently under investigation. This unusual redox chemistry has only been observed thus far with complex **6** in acetone solution.

A packing diagram of **7** is shown (Figure 1, right), highlighting a π-π interaction between a quinolyl ring fragment from one molecule and the ethynyl substituent of an adjacent molecule. The distance between the centroids of the quinolyl ring and the ethynyl triple bond is 3.499Å.

Table 2. Selected Bond Distances (Å) and Selected Bond Angles (deg) for **7**

bond	(Å)	angle	(deg)
Fe−O1	1.913(2)	O1−Fe−N1	163.96(9)
Fe−O2	1.915(2)	N2−Fe−N4	168.36(10)
Fe−N1	2.143(3)	N3−Fe−O2	163.02(10)
Fe−N2	2.130(2)	O1−Fe−O2	96.15(10)
Fe−N3	2.157(3)	O1−Fe−N2	87.50(9)
Fe−N4	2.141(3)	O2−Fe−N2	102.99(9)
C13−C17	1.462(5)	O2−Fe−N1	90.46(10)
C18−C19	1.430(5)	N2−Fe−N1	76.76(10)
C17−C18	1.177(5)	O1−Fe−N4	97.16(10)
C43−C47	1.450(4)	O2−Fe−N4	87.16(9)
C47−C48	1.181(4)	N1−Fe−N4	97.75(10)
C48−C49	1.450(5)	O1−Fe−N3	90.30(10)
		N2−Fe−N3	92.94(9)
		N1−Fe−N3	87.48(10)
		N4−Fe−N3	76.44(10)
		C18−C17−C13	175.9(4)
		C17−C18−C19	177.0(4)
		C48−C47−C43	176.5(4)
		C47−C48−C49	176.3(4)

To gain some insight into the structural properties of complexes **4**−**6**, we attempted to obtain X-ray powder diffraction patterns from these materials (Supporting Information, Figures S13−S15). While we could not obtain a profile from **4**, we managed to acquire some data for each of **5** (which is poorly crystalline) and **6**. In fact, the low angle powder data for **5** matches well with the calculated powder profile for **7**, suggesting that these complexes may share similar structural properties. The profile obtained from polycrystalline **6** is substantially different from both **5** and the calculated pattern for **7**, so no relationships can be drawn regarding the structural properties of this material.

Electronic Absorption Spectroscopy. In the visible region of the spectrum at 298 K, CH_2Cl_2 solutions of ligand **3** exhibit an absorbance maximum at 500 nm (ε = 285 M^{-1} cm^{-1}), the result of an intraligand charge transfer absorption (ILCT). At room temperature, darkly colored ethanol solutions of complexes **4**−**6** each exhibit LMCT bands at approximately 450 nm (ε = 4100 M^{-1} cm^{-1} for **6**). Cooling ethanol solutions of **4**−**6** in liquid nitrogen results in stark changes to the physical appearance of the solutions. We have performed absorption measurements (400−900 nm) at 77

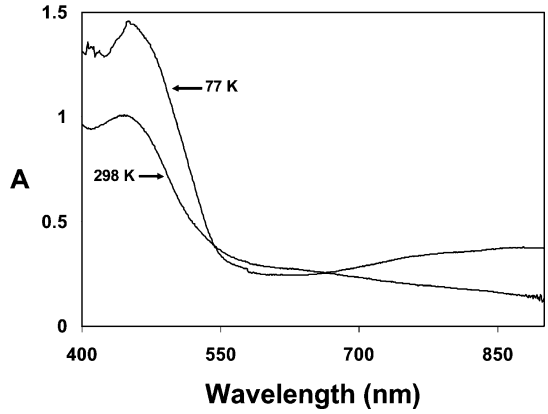

Figure 2. Visible spectra of **5** in ethanol solution at 298 K and as an ethanol glass at 77 K.

K for complexes **4**−**6** as ethanol glasses, and as a typical example, the spectra obtained for **5** at 298 and 77 K are shown in Figure 2. For each complex, there is a dramatic increase in absorbance of the LMCT band, as well as the appearance of a new broad absorption centered at approximately 850 nm.[14]

Electrochemistry. Cyclic voltammograms were obtained for compounds **3**−**6**, including voltammograms for unsubstituted QsalH (Supporting Information, Figure S13) and $[Fe(Qsal)_2]Cl$ (Supporting Information, Figure S12) reference compounds for comparison (to our knowledge there are no reported electrochemical studies on QsalH or any iron complexes of the Qsal anion). In the cathodic scan of **3** no reduction processes are evident until approximately −1.8 V (vs Fc), where an irreversible wave is present, which is also observed in the voltammogram of unsubstituted QsalH at a slightly more negative potential, and is likely an imine-centered reduction. An irreversible anodic process is observed at +0.0 V, which is also present in the voltammogram of unsubstituted QsalH, and likely represents oxidation of the hydroxyl group (Figure 3). The irreversible features observed at and past +0.4 V in the CV of **3** are also observed in the CV profile of unsubstituted QsalH. We believe that the thiophene oxidation potential occurs within, but is obscured by, this broad envelope of oxidations. To help corroborate this assignment a CV of precursor **2** was obtained, and a broad irreversible feature was observed at +1.2 V, which we attribute to thiophene ring oxidation.

In the CV of complexes **4** (Figure 3), **5** (Supporting Information, Figure S10), and **6** (Supporting Information, Figure S11), which are all very similar, the cathodic scan reveals a reversible Fe^{3+}/Fe^{2+} couple at −0.7 V followed by two pseudo-reversible reduction processes at −2.1 and −2.3 V, respectively, which represent reductions of the imine double bonds of each coordinated **3**. Over anodic potentials, irreversible features are observed at +0.7, +0.9 V, and 1.2 V that are also observed in the CV of $[Fe(Qsal)_2]Cl$ and represent oxidation of the Qsal ligand component. An extra irreversible feature centered at +0.3 V is noted in the CV of **5**, but not in the CV of $[Fe(Qsal)_2]Cl$, **4**, or **6**, and is ascribed to a thiocyanate-based oxidation process. For comparison, a CV of KSCN in acetonitrile shows an irreversible feature at about +0.2 V. Deconvolution of these waves was attempted using DPV. Over a potential of −1.0 V to +1.5 V, the voltammogram of $[Fe(Qsal)_2]Cl$ exhibits four broad waves, corresponding to the reduction and oxidation waves present in the CV. In complexes **4**−**6** four waves (five waves are observed with **5**) are noted over this region in the differential pulse voltammogram; however, the anodic wave centered at +1.2 V is much broader than that for $[Fe(Qsal)_2]Cl$. It is likely that the thiophene ring oxidation potential falls within this regime, overlapping with the Qsal oxidation, which is partly responsible for the broadness of the wave.

Repeated cycling (10 scans) between 0 and 1.5 V in each of **4**−**6** did not result in electropolymerization of the complexes as indicated by the lack of a significant increase in current with increasing number of cycles over this potential range and the absence of an electroactive film deposited on the working electrode following the experiment.[28] We surmise that the steric bulk of the $[Fe(Qsal)_2]^+$ substituent and high, irreversible thiophene oxidation potential are factors preventing the successful electropolymerization of these complexes. Electrochemical data for all compounds, including reference compounds, is summarized in Table 3.

Variable Temperature Magnetic Measurements, Mössbauer and EPR Spectroscopy. Magnetic susceptibility measurements were carried out with a SQUID magnetometer over the temperature range 2.5 (**4**) or 5 (**5**−**7**) − 325 K for complexes **4**−**7**. The data are displayed as plots of $\chi_M T$ versus T in Figure 4.

For complexes **4** and **6** spin-crossover from an $S = 5/2$ to an $S = 1/2$ state is clearly indicated by the decrease in $\chi_M T$ with decreasing temperature. The observed value of $\chi_M T$ for complexes **4** and **6** at 325 K (2.89 and 2.66 cm^3 mol K^{-1}, respectively) is less than the expected spin-only values for pseudo-octahedral coordinated high-spin iron(3+) (4.34 cm^3 mol K^{-1}), suggesting some proportion of low-spin component at this temperature. As temperature is decreased, a concomitant decrease in $\chi_M T$ is observed, and as temperature is raised from the lowest temperature of measurement, the $\chi_M T$ values observed are virtually identical to those recorded during the initial cooling. The profile of these data indicates that the spin-crossover in complexes **4** and **6** is best described as a gradual transition without thermal hysteresis, which is typical for iron(3+) complexes. At the lowest temperature of measurement (2.5 or 5 K) $\chi_M T$ values of 0.74 and 0.79 cm^3 mol K^{-1}, for complexes **4** and **6**, respectively, are observed, which are a little higher than the anticipated value for low-spin iron(3+) (0.375 cm^3 mol K^{-1}) but which are very typical values observed for other similar low-spin iron(3+) complexes of this kind.

Mössbauer spectra obtained at 293, 100, and 5.8 K for complex **4** mirror the variable temperature magnetic susceptibility data (Figure 5). At 293 K two sets of doublets with very different quadrupole splittings (QS) are observed, which is typical for similar iron(3+) complexes that exhibit gradual spin conversions. The inner doublet with QS of 0.66 mm/s and an isomer shift (IS) of 0.41 mm/s are assigned to

(28) Zhu, Y.; Wolf, M. O. *Chem. Mater.* **1999**, *11*, 2995–3001.

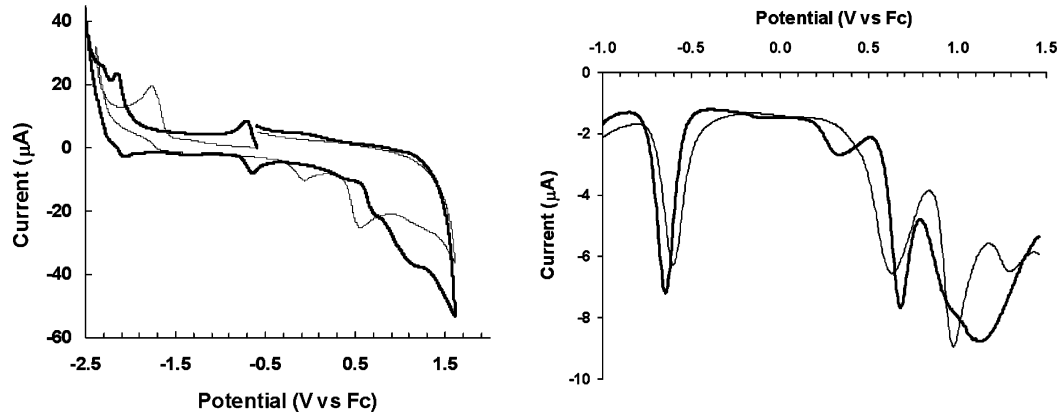

Figure 3. Left: Cyclic voltammograms of **3** (light trace) and **4** (bold trace) recorded in deaerated dichloromethane or acetonitrile solutions, respectively, containing 0.1 M $TEAPF_6$. Right: Differential pulse voltammograms for $[Fe(Qsal)_2]Cl$ (light trace) and **4** (bold trace).

Table 3. Electrochemical Data for Compounds **3**- **6** (Including Reference Compounds)

compound	E'_{ox} (V)	E'_{red}(V)
QsalH	+0.0, +0.6, +0.8	−1.9
[Fe(Qsal)$_2$]Cl	+0.7, +0.9, +1.3	−0.6, −2.0, −2.2
3	+0.0, +0.6	−1.8
4, **5**, and **6**	+0.3 (**5**), +0.7, +0.9, +1.2	−0.7, −2.1, −2.3

the high-spin isomer, in accordance with the magnetic data (Mössbauer data for complexes **4** and **5** can be found in Table 4). The outer doublet, with QS of 2.56 mm/s and IS of 0.14 mm/s, is assigned to the low-spin isomer. With decreasing temperature, the intensity of the inner doublet decreases with a concomitant increase in the intensity of the outer doublet,

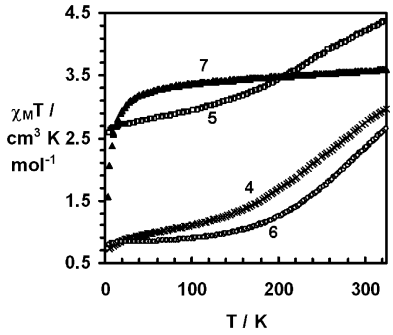

Figure 4. Temperature dependence of $\chi_M T$ value of **4** (×), **5** (□), **6** (○), and **7** (▲) (5000 Oe field).

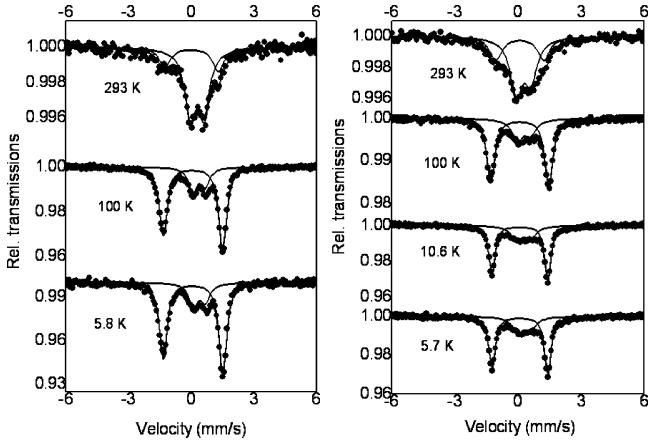

Figure 5. Temperature dependent Mössbauer spectra for **4** (left) and **5** (right). The dots represent the observed spectra; lines indicate simulated high-spin, low-spin, and the sum of high- and low-spin curves.

Table 4. Mössbauer Data for **4** and **5**[a]

T (K)	compound	IS (mm/s)	QS (mm/s)	site (%)	Fe(3+) spin state
293	**4**	0.41(1)	0.66(2)	73.6	5/2
		0.14(2)	2.56(4)	26.4	1/2
	5	0.38(1)	0.69(2)	66.5	5/2
		0.19(2)	2.28(4)	33.5	3/2
100	**4**	0.50(1)	0.61(2)	24.7	5/2
		0.200(1)	2.837(3)	75.3	1/2
	5	0.40(1)	0.61(2)	27	5/2
		0.203(2)	2.76(1)	73	3/2
10.6	**5**	0.37(1)	0.66(2)	30.5	5/2
		0.205(2)	2.649(3)	69.5	3/2
5.8	**4**	0.51(1)	0.58(2)	23	5/2
		0.201(2)	2.849(7)	77	1/2
5.7	**5**	0.41(2)	0.60(2)	29.3	5/2
		0.210(2)	2.649(4)	70.7	3/2

[a] The numbers in parenthesis are error bars obtained from the theoretical fittings to the experimental data.

which is the dominant absorption at 100 K. Between 100 and 5 K, the intensity ratio of the inner and outer doublets changes very little, and the QS for the outer doublet at 5 K is 2.849 mm/s, consistent with low-spin iron(3+).

The variable temperature magnetic data observed for **5** are different than the data observed with **4** or **6**. While the profile of the data is typical for iron(3+) spin-crossover complexes, and is similar to that observed for complexes **4** or **6**, the $\chi_M T$ values are anomalously high. Experiments were run very slowly to ensure thermal equilibrium at each point of measurement, and in triplicate for two independently prepared batches of the complex, and the data obtained in all cases were very similar. In **5**, the $\chi_M T$ values decrease gradually between 325 and 5 K. At 325 K, the $\chi_M T$ value (4.37 cm^3 mol K^{-1}) is significantly higher than the values observed with **4** or **6** at the same temperature and is consistent with high-spin iron(3+). Between 13 and 10 K, there is a very slight increase in $\chi_M T$, and magnetization versus field experiments at 5 K indicated no magnetic ordering for **5**, ruling out the possibility of a magnetic phase transition. Of note, the value of M_{sat} at 5.5 T (5 K) approaches 2.3 Nβ (Supporting Information, Figure S16), which is significantly higher than the expected value for low-spin iron(3+) (0.69 Nβ), but is, in fact, closer to the expected value for an $S = 3/2$ *intermediate* state (2.67 Nβ). Below 10 K, $\chi_M T$ continues to slowly decrease to a final value of 2.58 cm^3 mol K^{-1} at 5 K, which is significantly higher than the $\chi_M T$ values observed for **4** and **6** at similar temperatures,

but is much closer to the anticipated value for the $S = 3/2$ state (1.87 cm^3 mol K^{-1}) than a $S = 1/2$ state. Surprisingly, variable temperature magnetic susceptibility data from samples of compound **5** seem to suggest a thermally induced spin-crossover to an intermediate $S = 3/2$ state. While extremely rare, a similar observation was made very recently by Neya et al. with variable temperature magnetochemical, infrared, and Mössbauer studies on an azide complex of (2,7,12,17-tetrapropylporphycentato)iron(3+).[29,30] Ohgo has observed an unusual transition between $S = 3/2$ to 5/2 states in highly saddled iron(3+) porphyrin complexes by low temperature EPR studies.[31] To our knowledge, there are no other reported examples of non-porphyrin iron(3+) complexes that display a thermal equilibrium between $S = 5/2$ and $S = 3/2$ states.

In an attempt to help us understand this unusual magnetic behavior and to confirm an unusual $S = 5/2$ to $S = 3/2$ crossover in **5**, Mössbauer spectra were recorded on a freshly prepared sample of **5** at a variety of temperatures (Figure 5, right). The Mössbauer data at 293 K, like that recorded for complex **4**, indicate that complex **5** consists of spin isomers, with the high-spin isomer dominant at this temperature, displaying QS and IS values that are consistent with $S = 5/2$ iron(3+) (Table 4). Between 293 and 100 K, the intensity of the inner doublet decreases and the intensity of the outer doublet increases, very similar to the observations made with **4**, suggesting that a thermally induced spin-crossover is operative in **5**. At the lowest temperature of measurement (5.7 K), the QS value observed for the outer doublet (2.649 mm/s) is significantly less than the QS observed for compound **4** at the same temperature, which was ascribed to low-spin ($S = 1/2$) iron(3+) in conjunction with variable temperature magnetic susceptibility results. A QS of 2.649 mm/s is also completely consistent with the $S = 3/2$ state recently observed by Neya in an azide-substituted iron(3+) porphyrin complex.[29] It should be noted that many of the other iron(3+) porphyrin complexes that reportedly exhibit an intermediate spin state typically exhibit QS values that are greater than 3 mm/s.[32] However, from a structural and electronic point of view, complex **5** is significantly different from iron (3+) porphryin complexes, and we have no reason to assume that the Mossbauer properties of **5** will be similar. Also of note, the unusual feature noted in the magnetic data at approximately 10 K is mirrored in the Mössbauer spectrum at 10.6 K. Relative to the spectrum taken at 100 K, the intensity of the outer doublet decreases slightly, with a small increase in the intensity of the inner doublet also noted. Between 10.6 and 5.7 K, there is a very minor change in the relative intensities of the inner and outer doublets. We cannot rule out the possibility of a structural phase transition in the very low temperature regime, which results in an unusual but very small increase in high-spin isomer population. This unusual feature, however, does not detract from the clear observation of a thermally induced spin-crossover operative in **5**.

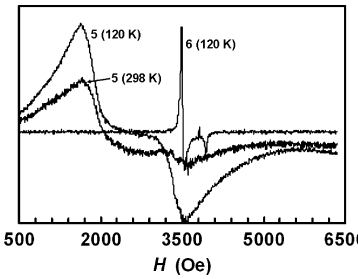

Figure 6. Powder EPR spectra of **5** at 298 K ($g = 4.03, 1.88$), 120 K ($g = 4.07, 1.89$), and **6** at 120 K ($g = 1.92, 1.71$).

Clear and unambiguous confirmation of an $S = 3/2$ state was provided by EPR spectroscopy on powdered samples of **5** at 298 and 120 K (Figure 6). At 298 K, a resonance at $g = 4.03$ is observed, which is characteristic for $S = 3/2$ systems. With decreasing temperature the intensity of the $g = 4$ resonance increases, suggesting, in accordance with the data from variable temperature magnetic susceptibility experiments, that the proposed $S = 5/2$ to $S = 3/2$ crossover is a true thermal equilibrium, with a distinct $S = 3/2$ intermediate state dominant at low temperature. For comparison purposes we ran an EPR experiment with complex **6** at 298 K but could not obtain a spectrum. At 120 K, however, a pseudoaxial spectrum is observed from **6** (Figure 6), which is typical for $S = 1/2$ systems, with no indication of a $g = 4$ resonance, indicating that the iron(3+) ion is in the low-spin state.

Taken together, the data from variable temperature magnetic, Mössbauer measurements, and EPR, provide strong evidence that a very unusual $S = 5/2$ to $S = 3/2$ crossover is operative in **5**. We are continuing to study the anomalous behavior of this complex.

With complex **7**, toward approximately 50 K, no significant temperature dependence or solid-state spin-crossover is evident from the magnetic data, which features iron(2+) in the high-spin state ($\chi_M T = 3.60$ cm^3 mol K^{-1} at 325 K). Below 50 K $\chi_M T$ begins to drop sharply, likely resulting from a combination of zero-field splitting of the high-spin state and weak intermolecular antiferromagnetic interactions. Close intermolecular π-π contacts were observed in the crystal packing of **7** (Figure 1).

The variable temperature magnetic properties of $Fe(Qsal)_2^+$ type complexes vary widely depending on the nature of the structure and counteranion present. In fact, completely high- and low-spin $Fe(Qsal)_2^+$ complexes have been reported with Cl^- and I^- counteranions, respectively; gradual spin-crossovers, like those described for complexes **4**−**6** containing the ThEQsal ligand have also been observed. Unusual abrupt transitions with hysteresis, while very uncommon in the magnetic properties of iron(3+) spin-crossover complexes, have also been observed with SCN^- and $SeCN^-$ counteranions. The demonstration of a thermally induced

(29) Neya, S.; Takahasi, A.; Ode, H.; Hoshino, T.; Hata, M.; Ikezaki, A.; Ohgo, Y.; Takahashi, M.; Hiramatsu, H.; Kitagawa, T.; Fururtani, Y.; Kandori, H.; Funasaki, N.; Nakamura, M. *Eur. J. Inorg. Chem.* **2007**, 3188–3194.
(30) Neya, S.; Takahashi, A.; Ode, H.; Hoshino, T.; Ikezaki, A.; Ohgo, Y.; Takahashi, M.; Furutani, Y.; Lorenz-Fonfria, V. A.; Kandori, H.; Hiramatsu, H.; Kitagawa, T.; Teraoka, J.; Funasaki, N.; Nakamura, M. *Bull. Chem. Soc, Jpn.* **2008**, *81*, 136–141.
(31) Ohgo, Y.; Chiba, Y.; Hashizume, D.; Uekusa, H.; Ozeki, T.; Nakamura, M. *Chem. Commun.* **2006**, 1935–1937.
(32) Nakamura, M. *Coord. Chem. Rev.* **2006**, *250*, 2271–2294.

crossover between $S = 5/2$ and $S = 3/2$ states in complex **5** is another example of interesting magnetic properties exhibited by complexes containing Qsal-type ligands.

Conclusions

Three iron(3+) spin-crossover complexes of the new ThEQsalH ligand were reported, including an example of a non-porphryin complex displaying a rare $S = 5/2$ to $S = 3/2$ crossover that we are currently investigating. These results have demonstrated that 3-ethynylthienyl substitution of the QsalH ligand is compatible with the iron complexes maintaining their spin-crossover properties. Unfortunately complexes **4**−**6** did not undergo electropolymerization, so we could not study the magnetic or conducting properties of any polymer films. However, we are actively pursuing the synthesis of other Qsal-type ligands containing substituents more amenable to electropolymerization reactions, such as terthiophene or ethylenedioxythiophene (EDOT). Work in this regard is underway and will be reported in due course.

Acknowledgment. The authors acknowledge financial support from the Natural Sciences and Engineering Research Council of Canada. M.T.L. thanks Brock University for providing start-up funds, Research Corporation for a Cottrell grant (No. CC6686), Prof. Melanie Pilkington for the use of electrochemistry equipment, and Dr. Prashanth Poddutoori for assistance with EPR experiments.

Supporting Information Available: FT-IR and ESI mass spectra of **4**−**6**, cyclic voltammograms for **3**−**6** and reference compounds, XPRD data for **5** and **6**, including the calculated pattern for **7**, magnetization data for **5**, and crystallographic data in CIF format. This material is available free of charge via the Internet at http://pubs.acs.org.

IC801233X